Large-Eddy Simulation of a multiple injector cryogenic combustor under transcritical conditions and large amplitude high frequency modulations

T. Schmitt, L Hakim, M. Boileau, G Staffelbach, A Ruiz, S. Ducruix, B. Cuenot, S. Candel

Large-Eddy Simulation of a multiple injector cryogenic combustor under transcritical conditions and large amplitude high frequency modulations

T. Schmitt[a,b,*], L. Hakim[a,b], M. Boileau[a,b], G. Staffelbach[c], A. Ruiz[c], S. Ducruix[a,b], B. Cuenot[c], S. Candel[a,b]

[a] CNRS, UPR 288, Laboratoire d'Energétique Moléculaire et Macroscopique, Combustion (EM2C), Grande Voie des Vignes, 92290 Châtenay-Malabry, France
[b] Ecole Centrale Paris, Grande Voie des Vignes, F-92290 Châtenay-Malabry, France
[c] Cerfacs, 42, Avenue Gaspard Coriolis, 31057, Toulouse Cedex 01, France

Abstract

The study focuses on the full simulation of a multiple coaxial configuration which typifies, on a model scale, the geometry and the thermodynamic and injection conditions found in real rocket engines. Cryogenic reactants (liquid oxygen and gaseous methane) are injected under transcritical conditions, a situation reached when the pressure is higher than the critical pressure of the reactants and the injection temperature is lower than the critical temperature. The dynamics of high-pressure transcritical flames submitted to high-frequency transverse acoustic modes is specifically considered. Calculations are carried out in the exact configuration of a model scale combustor mounted on the Mascotte cryogenic test bench (ONERA and EM2C), operating at 6.7 MPa. This system comprises five shear-coaxial injectors arranged on a line in the chamber backplane and it is equipped with a very high amplitude modulator (VHAM). This device periodically and alternately blocks the two exhaust nozzles of the combustion chamber, inducing a large amplitude transverse acoustic modulation. The flame region is then submitted to high amplitude transverse acoustic modes. The Large-Eddy Simulation (LES) flow solver AVBP from CERFACS and IFPEN is used in this work. The solver has been previously extended to handle high-pressure transcritical flows in a collaborative effort carried out by CERFACS and EM2C, CNRS. Results obtained by exploiting high-end computational resources demonstrate the feasibility of such calculations and provide insight in the process. The simulations highlight the mechanisms which can feed energy in the transverse mode and suggest possible descriptions of the driving processes. It is shown that calculations retrieve features found in experiments: the flames are more compact when they are made to interact with the transverse acoustic waves. The dense core length is notably reduced. The flames and dense cores are flattened in the spanwise direction, a feature which is also found in experiments. The unsteady motion observed experimentally is thus well obtained numerically. The transverse motion induced by the acoustic modulation is analyzed in detail. It is found that this motion closely follows the acoustic waves formed in the chamber in good agreement with a model proposed by Mery *et al.* [1].

Keywords: LES, flame dynamics, transcritical combustion, high-frequency combustion instability

1. Introduction

Combustion instabilities have often hindered developments of Liquid Rocket Engines (LRE). Such extreme dynamical phenomena were experienced in many high performance engines. It took a considerable amount of testing to eliminate high frequency instabilities arising in the F-1 of the Saturn V rocket [2]. Such instabilities were also encountered during the Ariane development program leading to the in-flight destruction of the second launcher on November 23, 1980. After a few seconds of operation high-frequency oscillations developed in the first stage propulsion system resulting in a rapid erosion and melting of the injection face due to the rapid intensification of heat fluxes under large amplitude oscillations of the thrust chamber parameters. Because this problem was so pervasive it has been extensively investigated. Most observations were made in real scale engines with relatively few model scale investigations. Theoretical understanding and experimental data based on large scale testing are summarized in [3] while more recent advances are reviewed in [4–6].

The present research project aims at advancing the state of the art in this field by exploring the possibilities of Large-Eddy Simulations (LES) with the following three objectives: (1) Check the numerical methodology by comparing the LES data to the experimental results, (2) Observe the dynamical response of coaxial flames in a high-frequency transverse acoustic field and complement experimental data and (3) Underline differences in flame dynamics depending on whether the flame is submitted to acoustic pressure or acoustic transverse velocity.

The simulations reported in what follows correspond to operating conditions prevailing in LREs reproduced in a multiple injector laboratory scale test configuration (MIC) equipped with an external actuator (designated as the VHAM). The VHAM induces large amplitude transverse acoustic modulations which interact with the multiple cryogenic flames established in the MIC. This device is fed with liquid oxygen injected in the central channels of coaxial injectors and this stream is surrounded by gaseous hydrogen or methane. The mean chamber pressure exceeds the critical pressure of the liquid oxygen ($p_c(O_2)$ = 5.04 MPa) which is injected at a temperature well below its critical value $T_c(O_2)$ = 154 K. Under these transcritical conditions, the working fluid state departs from that of a perfect gas [7], surface tension vanishes and mass transfer from the dense oxygen stream

*Corresponding author
Email address: thomas.schmitt@ecp.fr (T. Schmitt)

to the lighter surrounding stream is essentially governed by turbulent production of surface area and mixing. Combustion thus takes place in a complex flow featuring large density gradients and its simulation raises considerable physical and mathematical difficulties.

The flame structure under transcritical conditions is now well documented, for example in [8–11]. These data provide useful information for numerical modeling and have been used to guide simulation of transcritical flows. In the past decade, efforts have been made to establish computational methodologies for transcritical injection and combustion including real gas thermodynamics, transport models and modified algorithms for numerical integration. LES of turbulent transcritical jets and jet flames have been carried out in the transcritical range by different research groups ([12–20]). Much of this work has concerned coaxial flames formed by a transcritical oxygen stream surrounded by a high speed annular flow of hydrogen or methane. These simulations constitute the first step towards the simulations of more complex systems, representative of real engines.

The experimental configuration simulated in the present study has served in recent years to obtain an understanding of the driving and coupling processes in high-frequency instabilities. The Multiple-Injector Combustor (MIC), featuring five injectors representative of a LRE injection plane system, was conceived [1, 21], and mounted on the Mascotte cryogenic combustion facility of ONERA.

The simulations presented in this article reproduce the MIC equipped with the VHAM actuator that produces transverse acoustic modes in the chamber. The experimental setup is briefly described in Sec. 2. The LES solver and the numerical configuration used in the present investigation are reported in Sec. 3. Results are discussed in Sec. 4. Attention is focused on the flame motion induced by the transverse acoustic modulation.

2. Brief description of the simulated experimental setup

The experimental setup comprises a rectangular combustor featuring a backplane with five coaxial cryogenic injectors. This system is mounted on the Mascotte test-bench from ONERA [1]. The system operates at 6.7 MPa and liquid oxygen (LOx) is injected through the inner channel at 80 K. The LOx stream is surrounded by a high velocity flow of gaseous methane (GCH_4). The velocities of these LOx and GCH_4 streams are O(1) m.s^{-1} and O(100) m.s^{-1}, respectively. Under such conditions, representative of rocket engine steady state conditions of operation, the LOx is transcritical while GCH_4 is supercritical. The operating point conditions are gathered in Tab. 1.

The MIC is equipped with an actuator, known as the Very High Amplitude Modulator (VHAM) [1, 22], which was designed to generate extreme acoustic levels in the chamber in order to represent the pressure perturbations arising in combustion instabilities. This system is shown in Fig. 1. It consists of a toothed wheel that alternately blocks the two outlet nozzles of the chamber. The whole mass flow is thus ejected alternately from the top and bottom nozzles. For an appropriate rotation rate of the wheel corresponding to the transverse mode eigenfrequencies, strong resonances are induced in the chamber. Because the nozzles are shut by the wheel in an alternate fashion, transverse modes of odd order are promoted.

The MIC is equipped with large quartz windows that give access to the most of the flame region.

P_{ch}[MPa]	$\dot{m}_{LOx}$ [g.s^{-1}]	$\dot{m}_{CH_4}$ [g.s^{-1}]	MR	J
6.7	106	100	1.1	3.7

Table 1: Operating point chosen for the simulation. P_{ch} is the chamber mean pressure, $\dot{m}_{LOx}$ and $\dot{m}_{CH_4}$ are the mass flow rates of oxygen and methane, respectively. MR is the mixture ratio and J the momentum flux ratio. The injection temperatures are kept constant: T_{LOx} = 80K and T_{CH_4} = 288K.

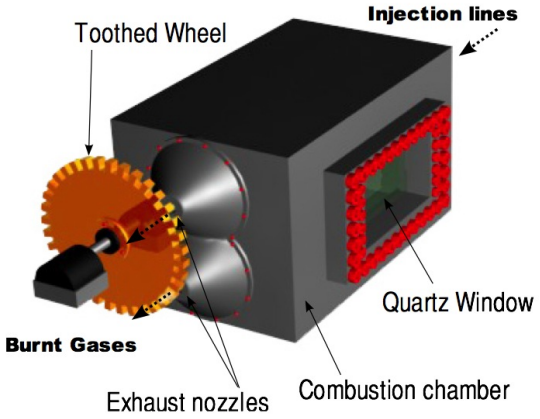

Figure 1: Schematic representation of the MIC equipped with the Very High Amplitude Modulator (VHAM) [23]

3. Numerical setup

3.1. Large-Eddy Simulation solver

The unstructured AVBP compressible flow solver (see among others [24, 25]) is used in what follows to integrate the three-dimensional compressible Navier-Stokes equations for a multi-component mixture of reactive fluids. The numerical method uses a low-dissipation centered scheme, third-order in space and time [26]. Boundary conditions are treated with the characteristic wave decomposition method NSCBC [27]. A real-gas version of the AVBP flow solver, called AVBP-RG, was recently developed [28, 29] with appropriate models to account for real-gas non-idealities. The Soave-Redlich-Kwong equation of state [30] was included in the solver:

$$p = \frac{\rho r T}{1 - \rho b_m} - \frac{\rho^2 a_m(T)}{1 + \rho b_m} \tag{1}$$

with T the temperature and $r = R/W$, where R designates the universal gas constant and W is the molar mass. The coefficients $a_m(T)$ and b_m are calculated according to [31]. Equation (1) is used for a consistent derivation of the pressure dependence of thermodynamic properties (internal energy, enthalpy, specific heats, compressibility), as described in [31, 32]. Chemical conversion is handled using an infinitely fast chemistry model presented in [20]. NSCBC boundary conditions are adapted to real-gas thermodynamics [33]. Because of the steep density and

internal energy gradients, real-gas simulations require a specific numerical stabilization procedure described in [29]. The WALE model [34] is used to represent the sub-grid scale (SGS) shear stress tensor. The SGS energy and species fluxes are modeled using gradient transport assumptions with sub-grid Prandtl and Schmidt numbers set to 0.7. Results of calculations in gaseous atmospheric pressure situations as well as in high pressure transcritical cases indicate that the AVBP-RG flow solver in combination with these models provides solutions which are in good agreement with experimental data. These partial validations indicate that one may use this code to examine transcritical combustion dynamics problems.

3.2. Numerical configuration

Calculations are carried out in the exact configuration (MIC+VHAM) used in the experimental investigation on the Mascotte test-bench. The mesh shown in Fig. 2 comprises 11,800,000 nodes and 63,300,000 cells. The number of cells used to represent the injector lips where the flame is anchored is equal to 6 which is reasonable in view of previous experience with similar calculations. Walls are treated with an adiabatic no-slip condition and an anisotropic turbulence is injected at the inlet following the methodology described in [35]. Bulk and rms profiles, resulting from an independent LES of a long tube with the same Reynolds number and mesh resolution, are used to impose velocity conditions of each injector. The MIC mean pressure is imposed using non-reflecting conditions at the two outlets.

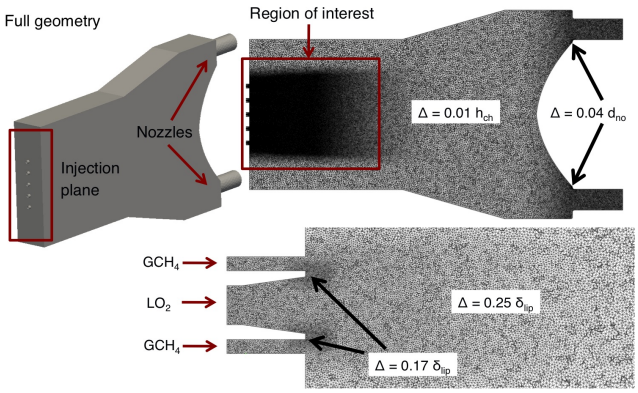

Figure 2: Full 3D geometry and mesh. Δ is the local cell size, d_{no} is the nozzle diameter and δ_{lip} and h_{ch} are the lip and chamber widths, respectively.

The acoustic perturbation generated by the VHAM is represented by an alternate modulation of the two outlets with an imposed pressure:

$$p'_{\mathrm{UP}} = A\sin(2\pi f t), \tag{2}$$

$$p'_{\mathrm{DOWN}} = A\sin(2\pi f t + \pi), \tag{3}$$

with A the amplitude of the modulation and f its frequency. The present study focuses on the 1T1L modulation (Fig. 3(a)). In this situation, flames are essentially modulated by a transverse acoustic velocity. Acoustic pressure fluctuations are zero for the center flame, and modulate the lateral flames. This approach allows to reach the modulation levels observed in the Mascotte experiments and recorded using dynamic pressure sensors located on the upper and lower side walls (Fig. 3(b)). The resulting acoustic modes suitably match the experimental data, as the frequency of modulation is successively made to coincide with the eigenfrequencies of the system.

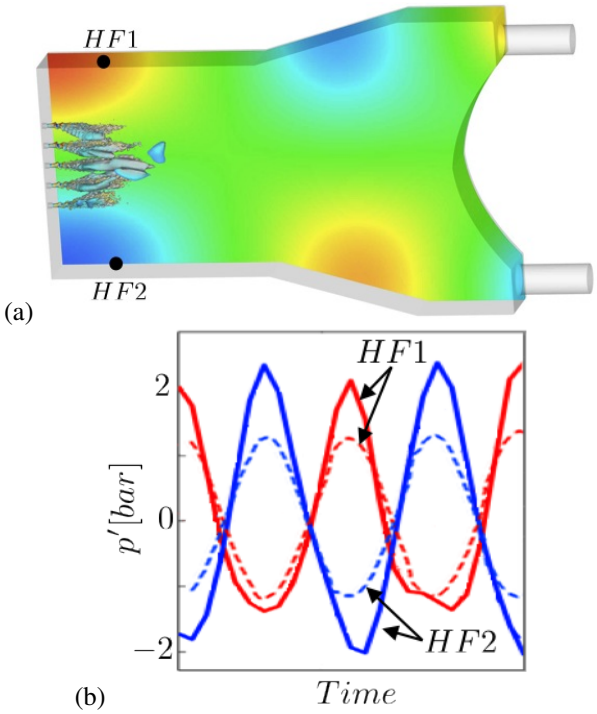

Figure 3: (a) Experimental (plain) and numerical (dashed) dynamical pressure signals recorded at HF1 and HF2. (b) 1T1L mode structure in the MIC. The five flames are represented by iso-surfaces of temperature (3000 K). The longitudinal slice shows an instantaneous pressure field (blue: 6.6MPa; red: 6.85MPa).

4. Results and discussion

Simulation results are first briefly described and then compared with experimental visualizations in Sec. 4.1. The discussion is then focused on the unsteady flame motion in Sec. 4.2.

4.1. Simulation results and comparison to experimental data

Flame structure

It is first convenient to examine cuts of the velocity amplitude (in red) together with density (greater than 100 kg.m^{-3}, in blue) shown in Fig. 4. In the absence of acoustic modulation, the typical transcritical flame geometry is observed [36]. The flame, localized between the oxygen and methane streams, has a limited spreading rate but extends far downstream in the chamber. This flame and the inner jet are strongly sheared by the high velocity gaseous annular flow. The latter quickly transitions to a fully turbulent flow. By opposition, the inner high density jet remains cohesive and penetrates up to 20 diameters into the chamber. Each flame is essentially axisymmetric (Fig. 4(a)) in this case.

As acoustic modulation is activated, the jets structure changes in a substantial fashion (Fig. 4(b)). The inner jet length is strongly reduced and alternate shedding of large scale vortices takes place in the annular gaseous stream. The methane jets are violently shaken by the transverse acoustic velocity generated by the modulation. The inner jets (and the flames) no longer remain axisymmetric, but are now flattened in the spanwise direction by the transverse velocity modulation.

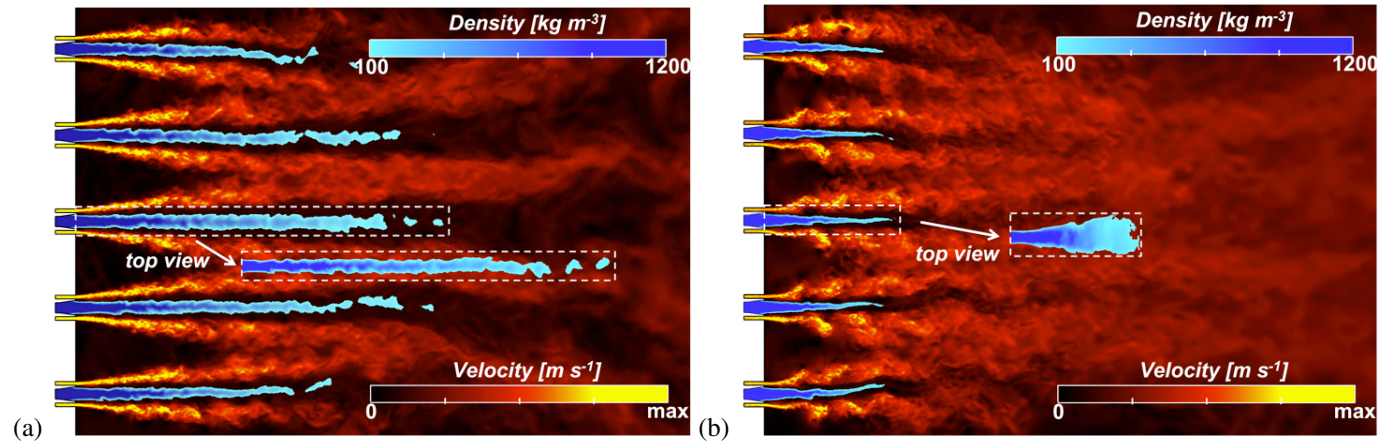

Figure 4: LES of the MIC featuring 5 injectors. Instantaneous longitudinal slice of density and velocity magnitude. (a) Without external acoustic modulation. (b) Submitted to a transverse acoustic modulation.

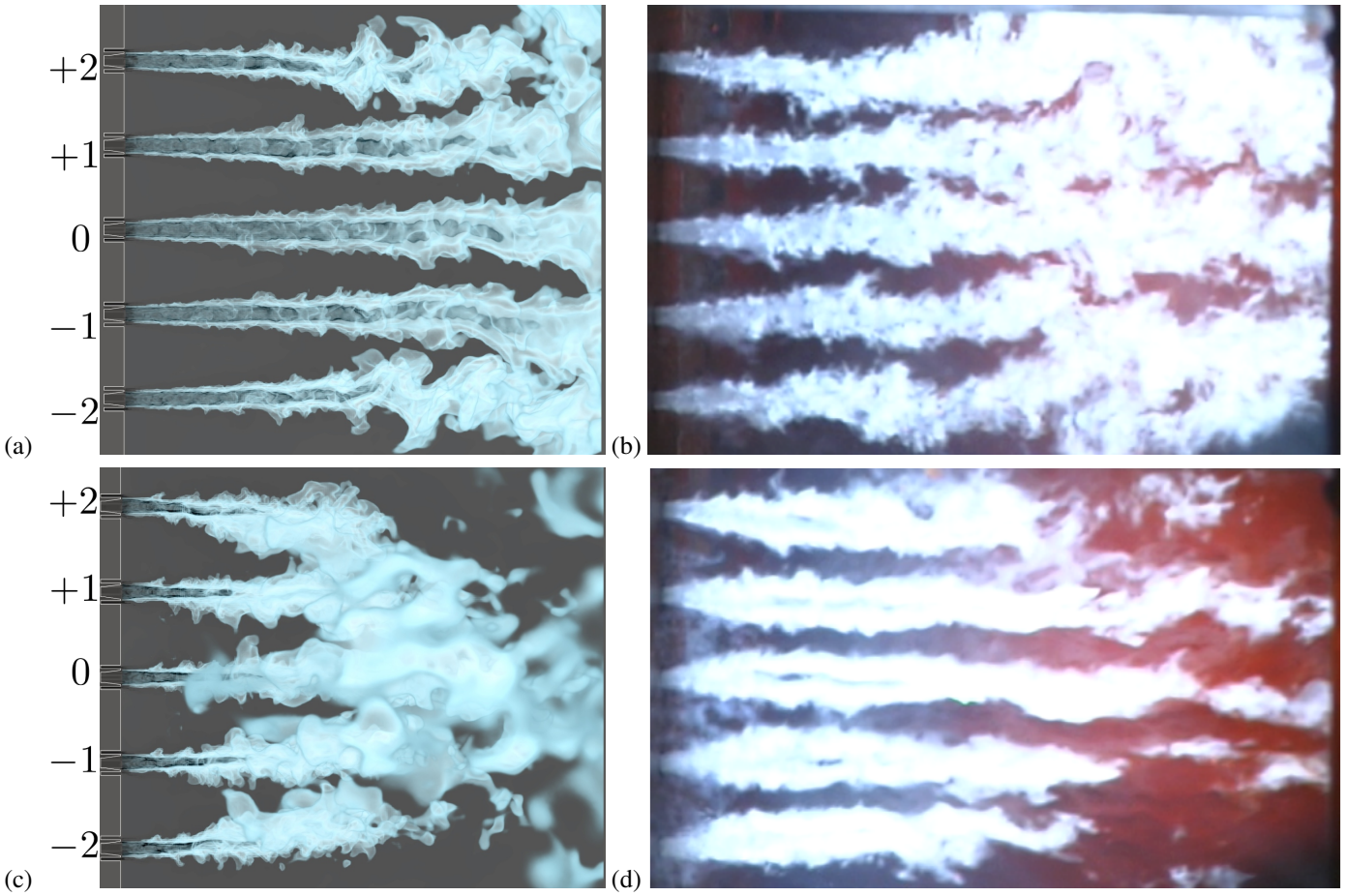

Figure 5: Left: Reconstructed emission images deduced from the simulations using a volume rendering of the temperature field (blue) and the density field (black) without modulation (a), with a 1T1L modulation (c) - Right: Experimental instantaneous visualizations of the flame light emission (b) without modulation, (d) with a 1T1L modulation.

Comparison with experimental visualizations

Figure 5 compares LES results to instantaneous visualizations from the experiment. Experimental images correspond to a direct view of the flames, which integrates the light emitted along the line of sight. This is qualitatively reproduced in the numerical results by using a volumetric rendering of the temperature field (in blue). The density field is also highlighted with a volumetric rendering in black. This comparison indicates that simulations are qualitatively able to retrieve what is observed experimentally, in terms of flame length and spreading rate. The two peripheral flames are slightly bent towards the chamber centerline. This is also visible in the experiments (Fig. 5(b)). This feature can be related to the formation of recirculation zones in the upper and lower left corners of the chamber and to a reduced pressure re-

gion in the center of the chamber.
When transverse acoustic perturbations are generated in the system (Fig. 5(c-d)), flames are shortened in both experiment and simulation. It is also found that the center flames are longer than the outer flames. The lateral flames bending towards the chamber centerplane is noticeably larger when the acoustic modulation is on. In Fig. 5(d), the dense cores become visible (dark region in the center of each flame) and two thick layers of intense luminosity form on their upper and lower sides. This phenomenon can be attributed to the flames flattening (Fig. 4). Both in the LES and in the experiments, the five flames oscillate as a block in the transverse direction following the transverse acoustic velocity. This aspect is investigated in details in Sec. 4.2.

4.2. Flames dynamics

Flame dynamics induced by the acoustic forcing is investigated in this section. In what follows, the analysis is based on phase averaged data. The different flames are referred as −2, −1, 0, +1 and +2 according to the corresponding injector transverse position (see. Fig. 6). It is proposed to analyze the dense oxygen jets motion as it is expected to drive the flames dynamics [37]. Each individual jet displacement is analyzed by plotting the jet transverse position y_0^i (where i is the flame number) for various phases of the acoustic modulation along the downstream direction. This position is defined as the transverse coordinate of the barycenter of the oxygen mass fraction profile.
Results for the center flame (flame 0) are shown in Fig. 6 (left). For $x < 10$d, one observes nearly sinusoidal oscillations. The inner jet shows little sensitivity to the transverse modulation. This flag-like motion is no longer visible further downstream. Instead, the jet features a up-down 'block' motion. The same behavior is noticed for the lateral flames. This is exemplified with flame +2 in Fig. 6(b). In addition to the transverse motion, lateral flames are also bent towards the center of the domain. This behavior is much more pronounced under acoustic modulation. Interestingly, it seems that this inclination is super-imposed to the transverse motion and does not alter its dynamics.

In an attempt to quantify the transverse flame displacement, spatially averaged position $\overline{y_0^i}(t)$ – relative to time average position – is computed over one period:

$$\overline{y_0^i}(t) \quad = \quad \frac{1}{x_2 - x_1} \int_{x_1}^{x_2} \left(y_0^i(x,t) - \left\langle y_0^i(x) \right\rangle \right) dx \qquad (4)$$

where $[x_1, x_2]$ is the interval of axial averaging and $\left\langle y_0^i(x) \right\rangle$ is the time average of $y_0^i(x,t)$. A first simple procedure is to perform the average over the whole flame length: $x_1 = 0$ and $x_2 = 25$d. The resulting values are plotted over time during one period in Fig. 7 (symbol ×), for flame 0 (a) and flame +2 (b). A harmonic motion, whose shape is similar to the mode shape induced by the acoustic modulation is clearly identifiable. Of interest is also the transverse position of the last part of the jet, the "block motion" region, defined by $x_1 = 15$d and $x_2 = 25$d. Results are gathered in Fig. 7 (symbol ∘) for both flames 0 and +2. As expected from Fig. 6, the amplitude of the transverse motion is larger in the second part of the jet, but differences between the two average intervals are limited. It is now interesting to compare these motions with the analytical model proposed by Mery *et al.* [1] to describe the flame movement induced by the transverse modulation.

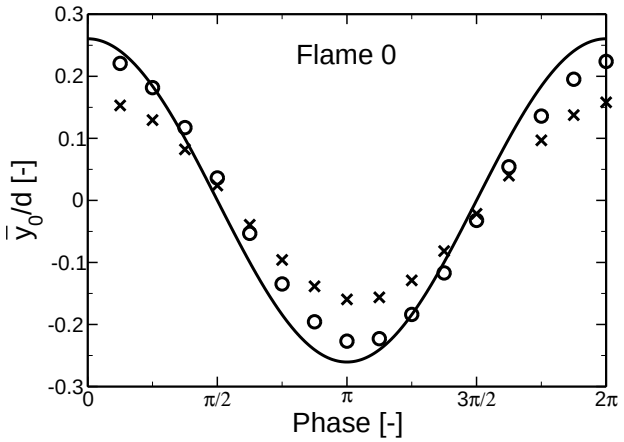

(a)

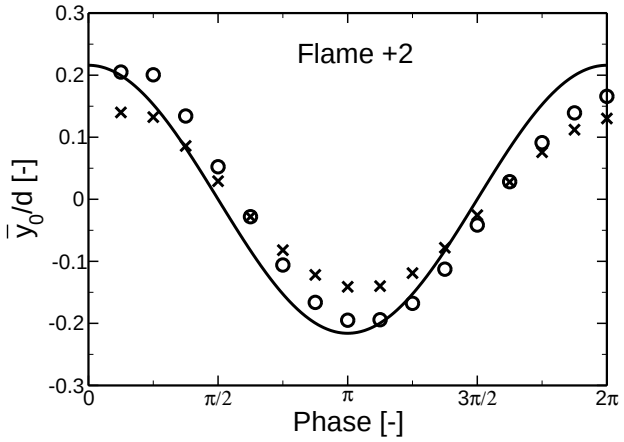

(b)

Figure 7: Theoretical and numerical flame displacement. — From Eq. 6; × Average flame position for $x < 25$d; ○ Average flame position for $15\text{d} < x < 25$d.

The model named FAME (Flame Acoustic Motion Equation) [1] has been deduced from experimental observations. It considers each flame as a thin line put set in motion by the transverse acoustic velocity. The flame transverse position in time is then estimated as a function of the transverse acoustic velocity. Under its simplest form, one can assume that the flame motion exactly matches the transverse acoustic motion. We suppose for simplicity a pure transverse mode here. The transverse acoustic velocity fluctuation is then independent of the axial position and is given by:

$$v'(y,t) \quad = \quad V \cos\left(\frac{\pi y_{fl}^i}{L}\right) \sin(\omega t) \qquad (5)$$

where v' is the transverse acoustic velocity generated by the modulation, V is the corresponding amplitude, y_{fl}^i is the initial position of flame i (i.e. the coordinate of the center of the injector), L the lateral dimension of the chamber, t the time and $\omega = 2\pi f$, with f the modulation frequency. Under the assumption that the transverse motion of the flame is small compared to the wavelength of the acoustic mode, the transverse displacement induced

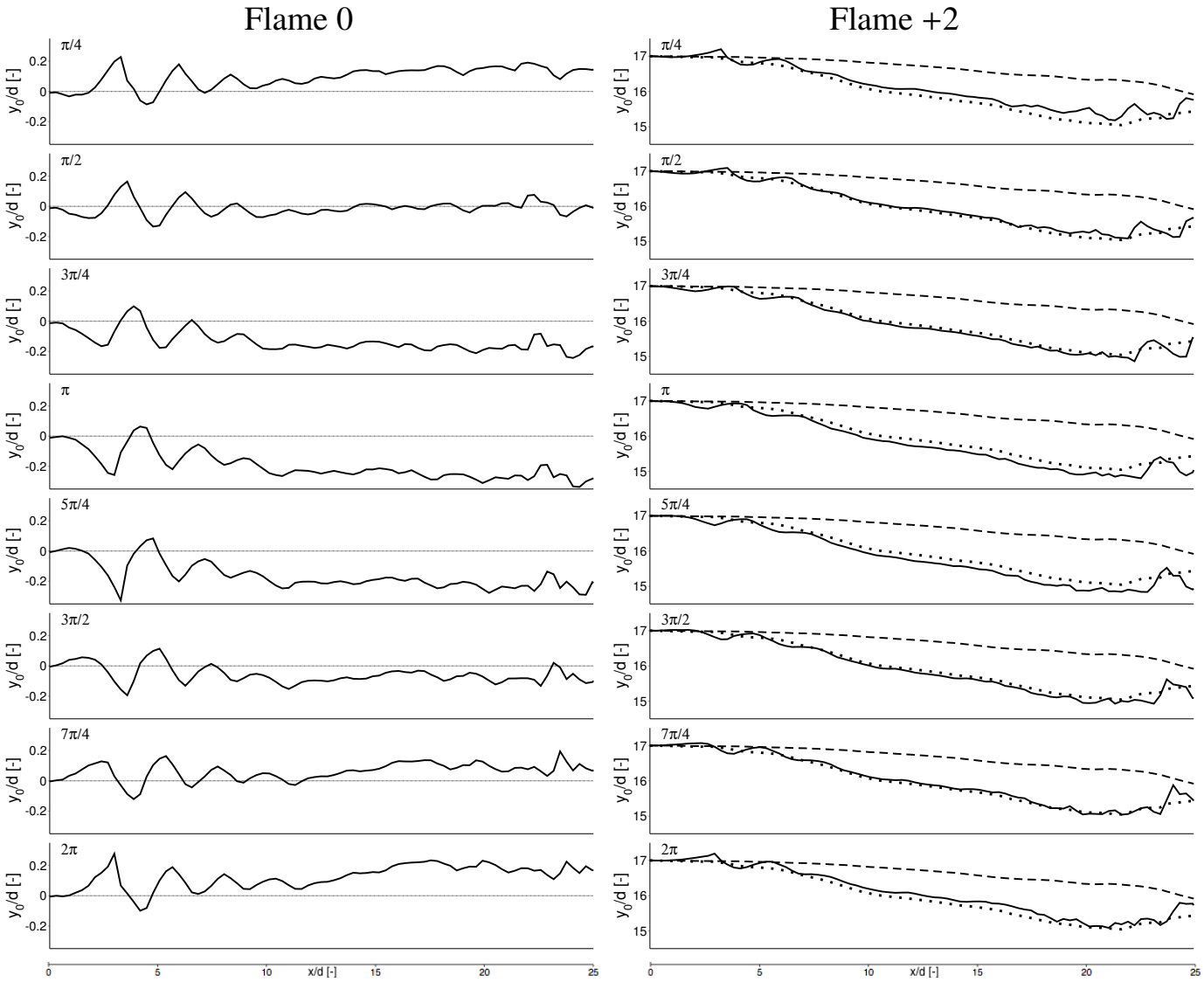

Figure 6: Longitudinal phase averaged profiles of oxygen jet transverse position for eight phases over one period. Left: flame 0; Right: flame +2. ── Under acoustic modulation; ─ ─ ─ Without acoustic modulation; · · · Average position under acoustic modulation

by acoustic is given by:

$$y_0^i(t) \quad = \quad y_{fl}^i + \frac{V}{\omega}\cos\left(\frac{\pi y_{fl}^i}{L}\right)\cos(\omega t) \tag{6}$$

One then obtains for flame 0:

$$y_0^0(t) \quad = \quad \frac{V}{\omega}\cos(\omega t) \tag{7}$$

and for flame +2:

$$y_0^{+2}(t) \quad = \quad y_{fl}^{+2} + \frac{V}{\omega}0.9563\cos(\omega t) \tag{8}$$

Equations 7 and 8 for flames 0 and +2 are plotted in Fig. 7 (continuous line). The model matches remarkably well the numerical results for both flames, indicating that the displacement model proposed by Mery *et al*. is able to properly account for the transverse motions executed by the flames when they are interacting with an imposed field of transverse acoustic velocity modulations.

5. Conclusion

This article reports results of Large Eddy Simulations (LES) of a multiple injector combustor mounted on the Mascotte cryogenic combustion test-rig. The MIC features 5 coaxial injectors forming a linear arrangement. This configuration is representative to some extent of real liquid rocket engines, and operates like these engines under transcritical conditions. The MIC is equipped with an acoustic actuator that produces transverse acoustic modulations, representative of a rocket engine instability. It is shown that calculations are able to retrieve experimental observations, both in presence or in absence of acoustic forcing. Under acoustic modulation, the flame lengths are notably reduced and the flames move in the transverse direction at the acoustic modulation frequency. Moreover, flames are flattened in the spanwise direction which nicely matches experimental observations. This phenomena explain the sudden changes in flame topology observed experimentally. The transverse flame displacement is investigated in detail. It is shown that a small amplitude flag-like motion is

present in the near injection region. Further downstream the jets move in "block". The flame transverse displacements are compared with the modeled approach suggested in Mery *et al.* [1]. In such a configuration the flames are supposed to follow the acoustic modulation field. Good agreement between simulations and the reduced model are obtained. On-going work deals with the analysis of a second simulation at higher frequency that corresponds to the 1T2L acoustic mode of the chamber. The calculations may also be employed to estimate the Rayleigh source terms which arise in the acoustic energy balance allowing a further discussion of the growth or decay of oscillations.

Acknowledgements

This work is supported by SAFRAN Snecma Space Engines Division, the prime contractor of the Ariane launcher cryogenic propulsion system, CNES and CNRS in the framework of the French-German program on Rocket Engines STability (REST). We acknowledge PRACE for awarding us access to resource Curie-TN based in France at TGCC, under the allocation 2010030367 - RA0367. The authors also thank P. Scouflaire and L. Vingert for their help during the experimental campaign.

References

[1] Y. Méry, L. Hakim, P. Scouflaire, L. Vingert, S. Ducruix, S. Candel, Compt. Rend. Mécan. 341 (2013) 100–109. Special issue "Combustion for Aerospace Propulsion".

[2] J. C. Oefelein, V. Yang, J. Propul. Power 9 (1993) 657–677.

[3] D. T. Harrje, F. H. Reardon, NASA Special Publication 194 (1972).

[4] V. Yang, W. Anderson (Eds.), Liquid Rocket Engine Combustion Instability, volume 169, Progress in Astronautics and Aeronautics, 1995.

[5] F. E. C. Culick, Unsteady Motions in Combustion Chambers for Propulsion Systems, volume RTO-AG-AVT-039 of *RTO AGARDograph*, The Research and Technology Organisation (RTO) of NATO, 2006.

[6] S. Candel, M. Juniper, G. Singla, P. Scouflaire, C. Rolon, Combust. Sci. Technol. 178 (2006) 161–192.

[7] J. Oefelein, Proc. Combust. Inst. 30 (2005) 2929–2937.

[8] M. Juniper, A. Tripathi, P. Scouflaire, J. Rolon, S. Candel, Proc. Combust. Inst. 28 (2000) 1103–1110.

[9] G. Singla, P. Scouflaire, C. Rolon, S. Candel, Proc. Combust. Inst. 30 (2005) 2921–2928.

[10] D. W. Davis, B. Chehroudi, J. Propul. Power 23 (2007) 364–374.

[11] K. Miller, J. Sisco, N. Nugent, W. Anderson, J. Propul. Power 23 (2007) 1102–1112.

[12] J. C. Oefelein, V. Yang, J. Propul. Power 14 (1998) 843–857.

[13] J. Oefelein, Combust. Sci. Technol. 178 (2006) 229–252.

[14] N. Zong, V. Yang, Combust. Sci. and Technol. 178 (2006) 193–227.

[15] N. Zong, V. Yang, Int. J. Computational Fluid Dynamics 21 (2007) 217–230.

[16] P. Tucker, S. Menon, C. Merkle, J. Oefelein, V. Yang, AIAA Paper 5226 (2008).

[17] G. Ribert, N. Zong, V. Yang, L. Pons, N. Darabiha, S. Candel, Combust. Flame 154 (2008) 319–330.

[18] M. Masquelet, S. Menon, Y. Jin, R. Friedrich, Aerospace Science and Technology 13 (2009) 466–474.

[19] S. Matsuyama, J. Shinjo, S. Ogawa, Y. Mizobuchi, in: 48th AIAA Aerospace Sciences Meeting, Orlando, Florida, pp. 2010–208.

[20] T. Schmitt, Y. Méry, M. Boileau, S. Candel, Proc. Combust. Inst. 33 (2011) 1383–1390.

[21] F. Richecoeur, P. Scouflaire, S. Ducruix, S. Candel, J. Propul. Power 22 (2006) 790–799.

[22] Y. Méry, Mécanismes d'instabilités de combustion haute-fréquence et application aux moteurs-fusées, Ph.D. thesis, Ecole Centrale Paris, 2010.

[23] Y. Méry, S. Ducruix, P. Scouflaire, S. Candel, Compt. Rend. Mécan. 337 (2009) 426–437.

[24] V. Moureau, G. Lartigue, Y. Sommerer, C. Angelberger, O. Colin, T. Poinsot, J. of Comput. Phys. 202 (2005) 710–736.

[25] N. Gourdain, L. Gicquel, M. Montagnac, O. Vermorel, M. Gazaix, G. Staffelbach, M. Garcia, J. Boussuge, T. Poinsot, Computational Science & Discovery 2 (2009) 015003.

[26] O. Colin, M. Rudgyard, J. Comput. Phys. 162 (2000) 338–371.

[27] T. Poinsot, S. Lele, J. Comput. Phys. 101 (1992) 104–129.

[28] L. Pons, N. Darabiha, S. Candel, Combust. Flame 152 (2008) 218–229.

[29] T. Schmitt, L. Selle, A. Ruiz, B. Cuenot, AIAA Journal 48 (2010).

[30] G. Soave, Chemical Engineering Science 27 (1977) 1197–1203.

[31] B. E. Poling, J. M. Prausnitz, J. P. O'Connel, The properties of gases and liquids, McGraw-Hill, fifth edition, 2001.

[32] V. Yang, Proc. Combust. Inst. 28 (2000) 925–942.

[33] N. Okong'o, J. Bellan, J. Comput. Phys. 176 (2002) 330–344.

[34] F. Nicoud, F. Ducros, Flow, Turbulence and Combustion 62 (1999) 183–200. JX.

[35] A. Smirnov, S. Shi, I. Celik, ASME Transactions- Journal of Fluids Engineering 123 (2001) 359–371.

[36] S. Candel, D. Durox, T. Schuller, N. Darabiha, L. Hakim, T. Schmitt, European Journal of Mechanics-B/Fluids (2013).

[37] L. Hakim, F. Richecoeur, P. Scouflaire, S. Ducruix, S. Candel, Submitted to Experiments in Fluids (2014).